Physics Letters B 809 (2020) 135776

Contents lists available at ScienceDirect

Physics Letters B

www.elsevier.com/locate/physletb

Variance in the radial distribution of nuclear matter between ^{56}Ni and ^{58}Ni inferred from a model-independent Sum-of-Gaussian analysis of elastic proton scattering data

X. Liu [a,b], P. Egelhof [b], O. Kiselev [b,*], M. Mutterer [b,1]

[a] Key Laboratory of Radiation Physics and Technology of the Ministry of Education, Sichuan University, Chengdu 610064, China
[b] GSI Helmholtzzentrum für Schwerionenforschung GmbH, 64291 Darmstadt, Germany

ARTICLE INFO

Article history:
Received 9 June 2020
Received in revised form 4 August 2020
Accepted 8 September 2020
Available online 11 September 2020
Editor: B. Blank

Keywords:
Nuclear radial matter density distribution
Model-independent Sum-of-Gaussians (SOG) method
Elastic proton scattering in inverse kinematics
Doubly magic radioactive ^{56}Ni nucleus

ABSTRACT

Differential cross sections for p-^{56}Ni and p-^{58}Ni elastic scattering, measured at low momentum transfer and at projectile energies of about 400 MeV/u with beams stored in the Experimental Storage Ring (ESR) at GSI, Darmstadt, have been analyzed up to $|t| = 0.06$ (GeV/c)^2 applying the model-independent Sum-of-Gaussians (SOG) method based on the Glauber multiple-scattering theory. The rms point matter radius of the self-conjugate doubly magic radioactive ^{56}Ni nucleus was deduced to be 3.62(6) fm, to be compared to the known radius of the stable ^{58}Ni nucleus, 3.67(7) fm. Although the radii of both nuclei differ only slightly, and there is close agreement of the matter radii of ^{58}Ni from former analyses using phenomenological parametrizations of the matter distribution, the SOG method was capable of elucidating pronounced differences in the shapes of the radial matter distributions between both nuclei. Consequences for the understanding of nuclear structure in the vicinity of the $N = Z = 28$ magic shell are briefly discussed.

The radial matter density distribution of the nucleus and the share of matter density between protons and neutrons are among the main topics in nuclear structure investigations, as they directly relate to the superposition of the squared wave functions of the two kind of nucleons [1]. Owing to their electric charge, the distribution of protons (nuclear charge) in a nucleus can be accurately measured by using leptonic probes such as for example elastic electron scattering, and is well known for many atomic nuclei [2]. As neutrons have no electric charge their density distribution is less easily accessible, i.e., via hadronic scattering [3], pion photoproduction [4], anti-protonic atom spectroscopy [5], and parity-violating electron scattering [6], etc. As for the distribution of total nuclear matter intermediate-energy elastic scattering of hadronic probes, predominantly protons and α-particles, has early become a powerful method [7–10]. The neutron density has also been frequently unraveled by subtracting proton densities from electron scattering experiments from matter densities deduced by hadronic scattering.

Such as the electrons in atoms, both the protons and neutrons in atomic nuclei occupy quantum levels by generating shells which are separated from each other by enhanced energy gaps. The amount of nucleons that completely fill the various shells define the so-called magic numbers, known as 2, 8, 20, 28, 50, 82, 126. Of special interest are the doubly magic nuclei with both protons and neutron concurrently occupying closed shells and, accordingly, being comparably strongly bound. Among them, in particular, self-conjugate, i.e., $N = Z$, nuclei are outstanding cases, such as the stable ^{4}He, ^{16}O and ^{40}Ca nuclei, and the radioactive ^{56}Ni nucleus, the latter being under study in the present work. An understanding of how magic configurations impact the nuclear charge, neutron and matter densities is among the main challenges of modern experimental and theoretical nuclear physics [11–13]. In recent years *ab initio* calculations of atomic nuclei have developed tremendously, permitting accurate modelling for the fundamental properties of light and medium-mass nuclei. The present work is devoted to an experimental study of the self-conjugate doubly magic ^{56}Ni nucleus which, constituting the same magic number 28 for both protons and neutrons, could possibly also be studied by *ab initio* methods. Indeed, theoretical predictions for the cross section of p-^{56}Ni elastic scattering at 400 MeV were recently presented [14]. Moreover the structure of ^{56}Ni plays also a pivotal role in nuclear

* Corresponding author.
E-mail address: O.Kiselev@gsi.de (O. Kiselev).
[1] M. Mutterer passed away in July 2019.

https://doi.org/10.1016/j.physletb.2020.135776

astrophysics, as it has been identified as one of the potential waiting point nuclei in the rapid proton-capture process powering type I x-ray bursts [15], and has a great impact in the stellar element synthesis in Super Nova type Ia outbursts [16].

The experiment, described in detail elsewhere [17–21], represents the first in-ring nuclear reaction experiment using stored radioactive beams interacting with internal targets at a storage ring, in the frame of the EXL project [22–25], namely elastic proton scattering on ^{56}Ni, performed in inverse kinematics at low momentum transfer. This new and challenging method enables to perform high-resolution measurements, even for very slow target-like recoil particles obtained from reactions at low momentum transfer, with reasonable luminosity [22,26]. For the present experiment, a 390.2 MeV/u ^{56}Ni beam was produced by fragmentation of a 600 MeV/u ^{58}Ni primary beam in the FRagment Separator (FRS), and then injected into and stored in the Experimental Storage Ring (ESR) at GSI Darmstadt for interacting with a H_2 gaseous jet target [27]. A remotely-controlled moveable aperture (optionally 1 or 2 mm width) was mounted in front of the target to permit considerable improvement in scattering angular resolution, and the energy and angle of the recoil protons were determined by a stack of DSSD and Si(Li) detectors housed in a specially designed pocket for separating them from the UHV of the ESR [20,25,28]. For comparison, elastic proton scattering from ^{58}Ni using a beam of stable ^{58}Ni at 400.1 MeV/u was measured under the same conditions. Under eikonal and adiabatic approximations, the matter root-mean-square (rms) radii R_m of ^{56,58}Ni were investigated by analyzing the measured differential cross sections $d\sigma/dt$ as a function of the Lorentz-invariant four-momentum transfer $-t$ [17,18] using the Glauber multiple-scattering theory [8,29]. By this method it has been demonstrated that from differential cross sections measured with high accuracy at low momentum transfer the overall nuclear size and radial shape of the nuclear matter density of exotic nuclei can reliably be determined [30–33]. A major drawback in the analyses of most of these previous experiments arises from the use of phenomenological model parametrizations for the nuclear matter density, such as a Fermi distribution. As in the case of inferring nuclear charge distributions from elastic electron scattering data, any kind of model parameters couple the matter density at various radii to each other making local density properties hard to derive [34]. It turns out that the matter radii obtained that way depend somewhat, albeit little, on the *a-priori* choice of one particular parametrization for the matter distribution. Usually a series of different phenomenological model functions were applied to reduce the model dependence and the variation of the results was used as indicator for the systematic uncertainty [30].

In the present work, we have used the model-independent Sum-of-Gaussians (SOG) method for analysing ^{56}Ni and ^{58}Ni elastic proton scattering, which originally was introduced [34] and successfully applied for deducing nuclear charge distributions from electron scattering data [2]. We are going to demonstrate that, although there is close agreement of the matter radii deduced from previous analyses using phenomenological parametrizations for modeling the nuclear matter distributions (see Table 1), the matter density distribution from the SOG method provides more abundant information on the nuclear structure, and only the SOG method is able to elucidate characteristic differences in the radial distribution of nuclear matter between both ^{56}Ni and ^{58}Ni nuclei.

In the SOG method, taking a vanishing first derivative at the origin, the nuclear matter density distribution, $\rho(r)$, for a given atomic nucleus is described by a summation of multi-Gaussian functions at arbitrary radii r_i ($r_i \in [0, R_{max}]$ fm) and with arbitrary amplitudes A_i as in [34]

$$\rho(r) = \frac{1}{2\pi^{3/2}\gamma^3}\sum_i^{N_g}\frac{A_i}{1+2R_i^2/\gamma^2} \times\left(\exp\left[-\frac{(r-r_i)^2}{\gamma^2}\right]+\exp\left[-\frac{(r+r_i)^2}{\gamma^2}\right]\right), \quad (1)$$

where $\rho(r)$ is normalised to the number of nucleons A as $4\pi\int\rho(r)r^2dr \equiv A$. In Eq. (1), γ is the common width of the Gaussians and N_g is the total number of Gaussians. The selection of γ, R_{max} and N_g was governed by the following constraints: (a) γ is limited by the finite nucleon size or by the smallest oscillatory structure from theoretical calculations [34]. Here, following Refs. [35–37], γ was taken as around 1.35 fm, which has been derived from various mean field (Hartree-Fock) radial wave functions for reproducing the tin and lead charge densities. (b) $R_{max} = 8$ fm was adopted following Ref. [34] from independent knowledge on the behavior of wave functions at large radii, that for these nuclei, the density tails at radii greater than 8 fm have a negligible contribution. (c) the minimum N_g was taken to be bigger than R_{max}/γ. Note that, although the limitations in γ, R_{max} and N_g are somewhat "arbitrary", their choice does not jeopardize the model independence of the resulting SOG density, since reasonably good physical arguments have been addressed as suggested in Ref. [34], and the values of γ and N_g were randomly varied around the start parameters in the following SOG analysis (see below).

For deducing the nuclear density distributions with the SOG method from the measured cross sections, again the Glauber multiple-scattering theory [29,8] was utilized. In the Glauber model, only the scalar part of the elementary proton-nucleon (pN) scattering amplitude was taken into account. Following Ref. [8], the scalar part of the elementary pN scattering amplitude was described by the standard high-energy parametrization with the total pN cross sections (σ_{pN}), the ratios of the real to the imaginary parts of the pN amplitudes (ϵ_{pN}) and the slope parameters (β_{pN}). For avoiding implementation of some model-dependence via the scattering amplitudes and for improving the accuracy of the Glauber calculations, σ_{pN}, ϵ_{pN} and β_{pN} were taken from experimental values. σ_{pN} and ϵ_{pN} were evaluated by MINUIT polynomial fits to the data from the Particle Data Group (PDG) [38], and Refs. [30,39], respectively. The β_{pN} values were assumed to be $\beta_{pp} = \beta_{pn}$ and were adjusted to give the best SOG description of the measured p-^{58}Ni cross section (Fig. 1) with the measured point matter rms radius 3.67(2) fm as average from four hadronic scattering measurements [40–43]. The above presented uncertainty for the radius was taken as the standard deviation of the mean values. Using the deduced effective β_{pN} value is considered to account, to some extent, for the spin effect which has not been explicitly treated in the present Glauber calculations such as in Refs. [8,30]. The input of the pN scattering amplitude used in the present work was: $\sigma_{pp} = 2.49(9)$ fm^2, $\sigma_{pn} = 3.31(8)$ fm^2; $\epsilon_{pp} = 0.53(5)$, $\epsilon_{pn} = 0.08(5)$; $\beta_{pp} = \beta_{pn} = 0.26(5)$ fm^2, for ^{56}Ni at 390.2 MeV/u, and $\sigma_{pp} = 2.54(9)$ fm^2, $\sigma_{pn} = 3.30(9)$ fm^2; $\epsilon_{pp} = 0.50(5)$, $\epsilon_{pn} = 0.06(5)$; $\beta_{pp} = \beta_{pn} = 0.26(5)$ fm^2, for ^{58}Ni at 400.1 MeV/u.

With the selected values for γ, R_{max} and N_g, and the obtained pN scattering amplitude, the free parameters of r_i and A_i can be deduced by a least-square fit of the calculated to the measured cross sections. In the present work, to reduce the number of parameters, r_i was first randomly distributed within 0-8 fm for each fit. Further, permitting a larger variability of the shape of the density distribution, γ and N_g were randomly varied in the fits, i.e., $\gamma \in [1.3, 1.4]$ fm, and $N_g \in [15, 25]$. During the fits, the pN scattering amplitude parameters were also randomly determined within their uncertainties. The parameters and the overall normalization factor were used as free parameters. Several thousand SOG fits were performed for ^{56}Ni, and ^{58}Ni, respectively. Note here that to

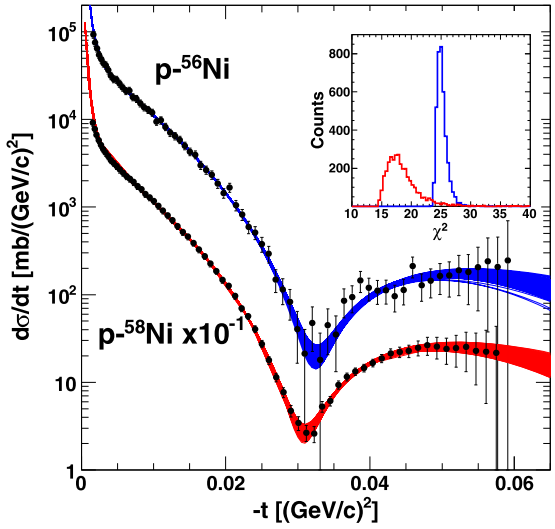

Fig. 1. Measured differential cross sections $d\sigma/dt$ as a function of the four momentum transfer squared $-t$ for p-^{56}Ni and p-^{58}Ni scattering at energies of 390.2 MeV/u, and 400.1 MeV/u, respectively. Data taken with a 1 mm wide aperture [17,18] are shown. The measured differential cross section of p-^{58}Ni is divided by a factor of 10. The bundle of solid lines corresponds to all "good" fits within the framework of the Glauber multiple-scattering theory using SOG distributions for describing the matter densities. The insert shows the probability histograms of the resulting χ^2 values for ^{56}Ni, and ^{58}Ni, respectively.

minimize fitting uncertainties due to the relatively large error bars of the measured cross sections at large momentum transfer, the fitting window was chosen only up to $|t| = 0.06$ (GeV/c)^2 for both nuclei. As demonstrated in the insert of Fig. 1, good fits form a sharp peak at the low value side of the χ^2 probability histogram and were selected according to the criterion of having a χ^2 smaller than 28 for ^{56}Ni, and 25 for ^{58}Ni, respectively. All selected fits are presented as the two bundles of solid lines for the two isotopes in Fig. 1. The measured cross sections are described by these fits rather well. Each fit which contributes to the bundles corresponds to one unique point matter rms radius and one point matter density distribution. The matter rms radius and density distribution were finally deduced by averaging the results from all these fits with an equal weight.

The present results for the matter rms radii of ^{56}Ni and ^{58}Ni are presented in Table 1 together with results of former analyses of the current data and those from earlier experiments, which predominantly applied model-dependent methods. The overall errors of the present matter rms radii include contributions (a) due to the experimental uncertainties in geometry and counting statistics (0.05 fm for ^{56}Ni and 0.06 fm for ^{58}Ni, respectively), and (b) due to the uncertainties of the SOG fitting procedure including uncertainties of the γ-N_g randomization, and the uncertainties of the pN scattering amplitude parameters (0.02 fm for both ^{56}Ni and ^{58}Ni). The present values for both nickel isotopes are within errors consistent with the majority of former model-dependent analyses, demonstrating minor sensitivity of the matter rms radii on the various assumed distributions used for describing the nuclear matter density. In recent work, the structure of ^{58}Ni has been used to calibrate so-called medium effects in the analysis of proton scattering on heavier nuclei (such as Sn [48] and Pb [3] isotopes). ^{58}Ni serves here as reference since its proton and neutron density distributions are nearly the same, and also the proton and neutron rms radii coincide. The present work includes the total matter distribution in ^{58}Ni evaluated reliably by the SOG method, while the corresponding charge distribution is available with good accuracy from elastic electron scattering [2].

The radial matter density distributions deduced in the present analysis are plotted in Fig. 2, with shaded bands representing the

Table 1
Point nuclear matter radii R_m (in fm) for ^{56}Ni and ^{58}Ni, compared with results from model-dependent analyses. ([a]Present work with total errors. [b]Other results from model-dependent analyses. For some of these results the relatively small errors are most probably due to an incomplete error investigation.)

^{56}Ni	3.62(6)[a]	3.66(8) [17][b]	
^{58}Ni	3.67(7)[a]	3.65(5) [40][b]	3.63(3) [44][b]
	3.67(10) [45][b]	3.68(3) [41][b]	3.67(7) [46][b]
	3.70(8) [47][b]	3.66(10) [42][b]	3.70(7) [43][b]
	3.69(9) [17][b]		

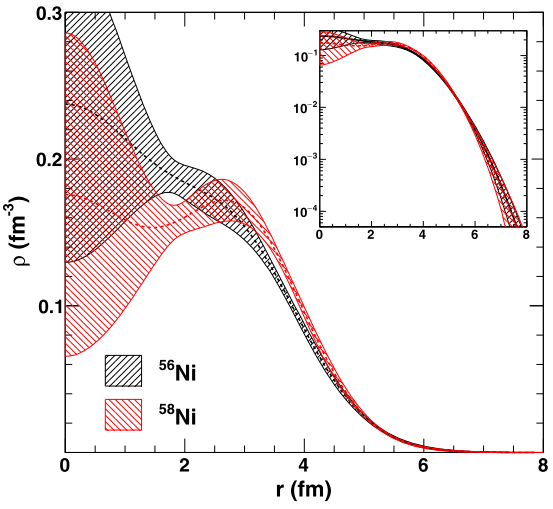

Fig. 2. Point nuclear matter density distributions deduced from the experimental cross sections of p-^{56}Ni (black) and p-^{58}Ni (red) elastic scattering using the SOG method. The dashed lines represent the mean distributions deduced; the shaded error bands relate to the errors from the standard deviation at given radii. The insert shows the same data, but with a logarithmic scale along the density-axis.

uncertainties at given radii. In spite of the close agreement of the matter rms radii from the SOG and model-dependent analyses for both nickel isotopes (see Table 1), their matter density distributions differ from most of those obtained in former analyses using model-dependent parametrizations for the description of the density distributions (see references in Table 1). In particular, it is interesting to observe significantly different shapes of the matter density distributions between ^{56}Ni and ^{58}Ni, in spite of the rather wide error bands at low radius values due to the limitation of the experimental data to low-momentum transfer. The density distribution of ^{56}Ni from the present SOG analysis overall decreases as r increases, with a hint to a small hillock around 2.5 fm. In contrast, the matter distribution of ^{58}Ni at first clearly passes a shallow minimum around 2.0 fm and a local maximum below 3.0 fm before decreasing. The nuclear densities then decrease rapidly in both cases as r approaches and exceeds the average nuclear sizes. Compared to ^{58}Ni, the nuclear density at the surface is a bid smaller in ^{56}Ni, and the surface diffuseness (defined as density values from 10% to 90% of the descent) is a bid larger, best seen using the logarithmic scale (see insert of Fig. 2). There are a few results of a model-independent analysis published for 1 GeV elastic proton scattering on ^{58}Ni and other nuclei [49,50], yielding a shape of the matter density distribution in close agreement with the present work. It is worth mentioning that various theoretical calculations, i.e. the relativistic Hartree-Fock-Bogoliubov (RHFB) calculation of Li et al. [51], also show a slightly fluctuating structure in the ^{58}Ni density, supporting the finding of the present work.

The study of the β-unstable ^{56}Ni and adjacent nuclei in the nuclide chart may provide valuable insight into the structure of

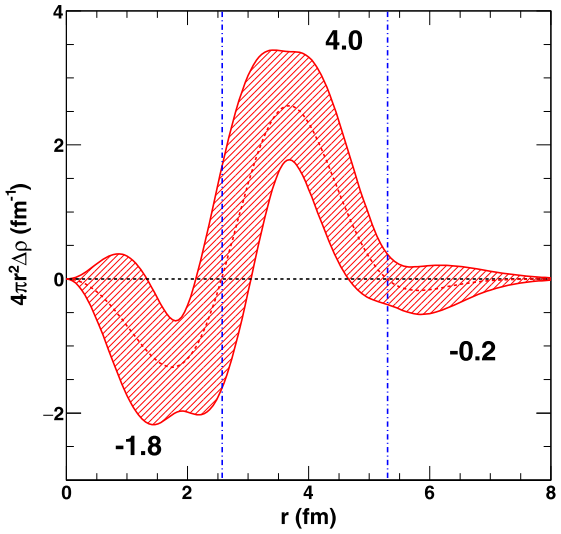

Fig. 3. Difference of the deduced point nuclear matter density distributions of ^{58}Ni and ^{56}Ni, multiplied with $4\pi r^2$. The dashed line in the middle of the shaded error band represents the mean density difference. The numbers refer to the deficit or the excess of the nucleon number.

unstable systems even further away from stability. In a sense, ^{56}Ni exhibits a more compact structure compared to that of ^{58}Ni. A similar compact structure has also been observed for the model-independent density distributions of the lighter doubly magic self-conjugate nucleus ^{40}Ca deduced from previous proton and alpha scattering experiments [35,52], and more oscillating densities were found there for ^{42}Ca and for the more neutron rich Ca isotopes. The present observation suggests that instead of increasing the surface diffuseness from ^{56}Ni to ^{58}Ni by the addition of a neutron pair to a ^{56}Ni core there are obviously significant core rearrangement effects, finally causing also the relatively small rms matter difference of 0.05(10) fm between both nuclei (see Table 1).

This becomes even more obvious by investigating the difference in the deduced matter density distributions between ^{56}Ni and ^{58}Ni, shown in Fig. 3. Of particular interest is the pronounced oscillating structure observed here. Also this result reflects a significant core rearrangement effect from ^{56}Ni to ^{58}Ni by adding two valence neutrons outside the $f_{7/2}$ shell closure. From $r = 0$ fm to the zero-crossing at $r = 2.6$ fm, about 1.8 nucleons are found to be transferred from the inner core to the further outside surface, summing up with the additional two neutrons for ^{58}Ni to an excess of 4.0 nucleons. According to a detailed shell-model study of the ground and excited states of nuclei around ^{56}Ni of Honma et al. [13], the probability of the closed $\pi(f_{7/2})^8\nu(f_{7/2})^8$ configuration is postulated to be 68% in ^{56}Ni, being larger than a value of 57% obtained with an assumed $\pi(f_{7/2})^8\nu(f_{7/2})^8$ core in ^{58}Ni. Our finding favorably compares with the difference of about 1.8 nucleons estimated from the full $\pi(f_{7/2})^8\nu(f_{7/2})^8$ occupancy difference (11% of 16 nucleons of the $f_{7/2}$ shell). The $f_{7/2}$ shell occupancy difference could therefore explain the difference in the density distribution between both nickel isotopes obtained from the present work. Similarly, an interior rearrangement of protons from the core was found in investigating charge density differences among stable nickel isotopes $^{58-64}$Ni, analyzed from elastic electron scattering with the aid of a model-independent SOG analysis (see Fig. 4 of Ref. [53]). On average about 0.5 protons are attracted and moved outside beyond $r = 4$ fm with adding each additional neutron pair. There is a good reason to believe that between ^{56}Ni and ^{58}Ni also a rearrangement of protons from the core may occur with some probability. In the present work, an indication of such rearrangement effects in the matter distributions of the ^{56,58}Ni nuclei was obviously only possible to work out with the SOG analyzing method which is able to reveal local density variations due to its model independence.

In summary, differential cross sections $d\sigma/dt$ for elastic proton scattering on ^{56}Ni and ^{58}Ni, measured in inverse kinematics and at low-momentum transfer at the ESR at GSI Darmstadt, were analyzed using the Glauber multiple-scattering theory applying the model-independent Sum-of-Gaussians (SOG) method. The rms radii of both nuclei differ only slightly but, because the SOG method is a valuable method for verifying local density variations, significantly different radial shapes of the matter density distributions between both nuclei could be observed. In ^{56}Ni, the nuclear matter density distribution exhibits a more compact structure as compared to that of ^{58}Ni. The difference in the matter density distributions between both nuclei suggests a significant core rearrangement effect from ^{56}Ni to ^{58}Ni by adding two neutrons outside the $f_{7/2}$ shell closure, in agreement with extended shell model investigations on the stability of the doubly closed $f_{7/2}$ shell in ^{56}Ni. In the past, similar core rearrangement effects were found for nuclear charge densities among stable nickel isotopes by analyzing elastic electron scattering data with the aid of the SOG analysis [53]. The exploration of nuclear charge density distributions in radioactive nuclei such as ^{56}Ni may soon also be possible using the SCRIT facility at the RIKEN radioactive isotope (RI) factory [54] or ELISE at the future NUSTAR facility at FAIR [55]. Then the neutron densities of radioactive nuclei could be inferred from unfolding proton from matter densities, both determined using SOG analyses. The perspective of attaining valuable insight into *exotic* neutron structures in radioactive nuclei, e.g., skin or halo structures [56] and predicted central-bubble structures [57] may also become accessible.

Declaration of competing interest

Authors are stating there is no conflict of interests.

Acknowledgements

We thank G.D. Alkhazov and A.V. Dobrovolsky (PNPI, Gatchina) and T. Neff (GSI) for fruitful discussions about the Glauber theory and the data analysis. This research was supported by the National Natural Science Foundation of China (No. 11705242).

References

[1] G. Hagen, et al., Nat. Phys. 12 (2016) 186.
[2] H. de Vries, C.W. de Jager, C. de Vries, At. Data Nucl. Data Tables 36 (1987) 495.
[3] J. Zenihiro, et al., Phys. Rev. C 82 (2010) 044611.
[4] C.M. Tarbert, et al., Phys. Rev. Lett. 112 (2014) 242502.
[5] A. Trzcińska, et al., Phys. Rev. Lett. 87 (2001) 082501.
[6] S. Abrahamyan, et al., Phys. Rev. Lett. 108 (2012) 112502.
[7] A.N. Antonov, et al., Phys. Rev. C 72 (2005) 044307.
[8] G.D. Alkhazov, S.L. Belostotsky, A.A. Vorobyov, Phys. Rep. 42 (1978) 89.
[9] C.J. Batty, et al., Adv. Nucl. Phys. 19 (1989) 1.
[10] H. Sakaguchi, J. Zenihiro, Prog. Part. Nucl. Phys. 97 (2017) 1.
[11] R.F. Garcia Ruiz, et al., Nat. Phys. 12 (2016) 594.
[12] A. Ekström, et al., Phys. Rev. C 91 (2015) 051301.
[13] M. Honma, et al., Phys. Rev. C 69 (2004) 034335.
[14] M. Vorabbi, P. Finelli, C. Giusti, Phys. Rev. C 98 (2018) 064602.
[15] C. Langer, et al., Phys. Rev. Lett. 113 (2014) 032502.
[16] E. Churazov, et al., Nature 512 (2014) 406.
[17] M. von Schmid, Nuclear matter distribution of ^{56}Ni measured with EXL, Ph.D. Thesis, TU Darmstadt, 2015, http://tuprints.ulb.tu-darmstadt.de/5028.
[18] M. von Schmid, et al., submitted to Nature.
[19] P. Egelhof, et al., JPS Conf. Proc. 6 (2015) 020049.
[20] M. Mutterer, et al., Phys. Scr. T 166 (2015) 014053.
[21] M. von Schmid, et al., Phys. Scr. T 166 (2015) 014005.
[22] FAIR Baseline Technical Report, H.H. Gutbrod, et al. (Eds.), 2006, ISBN-3-9811298-0-6.
[23] B. Rubio, T. Nilsson, Nucl. Phys. News 16 (1) (2006) 9.
[24] O. Kiselev for the EXL Collaboration, Phys. Scr. T 166 (2015) 014004.

[25] P. Egelhof for the EXL Collaboration, Accepted for publication in proceedings of the 10th international conference on nuclear physics at storage rings, in: JPS Conf. Proc., 2020.
[26] P. Egelhof, et al., Phys. Scr. T 104 (2003) 151.
[27] M. Kühnel, et al., Nucl. Instrum. Methods A 602 (2009) 311.
[28] B. Streicher, et al., Nucl. Instrum. Methods A 654 (2011) 604.
[29] R.J. Glauber, in: W.E. Brittin, L.G. Dunham (Eds.), Lectures in Theoretical Physics, Vol. 1, Interscience, New York, 1959, p. 315.
[30] G.D. Alkhazov, et al., Nucl. Phys. A 712 (2002) 269.
[31] P. Egelhof, et al., Eur. Phys. J. A 15 (2002) 27.
[32] A.V. Dobrovolsky, et al., Nucl. Phys. A 766 (2006) 1.
[33] S. Ilieva, et al., Nucl. Phys. A 875 (2012) 8.
[34] I. Sick, Nucl. Phys. A 218 (1974) 509.
[35] L. Ray, Phys. Rev. C 19 (1979) 1855.
[36] J. Cavedon, et al., Phys. Lett. B 118 (1982) 311.
[37] B. Frois, et al., Phys. Rev. Lett. 38 (1977) 152.
[38] C. Patrignani, et al., Particle Data Group, Chin. Phys. C 40 (2016) 100001 and 2017 update.
[39] L. Ray, Phys. Rev. C 20 (1979) 1857.
[40] G.D. Alkhazov, et al., Phys. Lett. B 67 (1977) 402.
[41] G.S. Blanpied, et al., Phys. Rev. Lett. 39 (1977) 1447.
[42] I. Brissaud, et al., Nucl. Phys. A 191 (1972) 145.
[43] J.C. Zamora, et al., Phys. Rev. C 96 (2017) 034617.
[44] A. Chaumeaux, V. Layly, R. Schaeffer, Phys. Lett. B 72 (1977) 33.
[45] R.M. Lombard, G.D. Alkhazov, O.A. Domchenkov, Nucl. Phys. A 360 (1981) 233.
[46] L. Ray, et al., Phys. Rev. C 18 (1978) 1756.
[47] G.W. Hoffmann, et al., Phys. Lett. B 79 (1978) 376.
[48] S. Terashima, et al., Phys. Rev. C 77 (2008) 024317.
[49] V.E. Starodubsky, V.R. Shaginyan, Yad. Fiz. 30 (1979) 55;
V.E. Starodubsky, V.R. Shaginyan, Sov. J. Nucl. Phys. 30 (1979) 28.
[50] J. Streets, B.A. Brown, P.E. Hodgson, J. Phys. G, Nucl. Phys. 8 (1982) 839.
[51] J.J. Li, W.H. Long, J. Margueron, N.V. Giai, Phys. Lett. B 788 (2019) 192 and private communication.
[52] H.J. Gils, E. Friedman, Z. Majka, H. Rebel, Phys. Rev. C 21 (1980) 1245.
[53] H.D. Wohlfahrt, et al., Phys. Rev. C 22 (1980) 264.
[54] T. Ohnishi, et al., Phys. Scr. T 166 (2015) 014071.
[55] T. Suda, H. Simon, Prog. Part. Nucl. Phys. 96 (2017) 1.
[56] I. Tanihata, H. Savajols, R. Kanungo, Prog. Part. Nucl. Phys. 68 (2013) 215.
[57] A. Mutschler, et al., Nat. Phys. 13 (2017) 152.